

Control of Host-Matrix Morphology Enables Efficient Deep-Blue Organic Light-Emitting Devices

Haonan Zhao, Jongchan Kim, Kan Ding, Mina Jung, Yongxi Li, Harald Ade, Jun Yeob Lee, and Stephen R. Forrest*

Mixing a sterically bulky, electron-transporting host material into a conventional single host–guest emissive layer is demonstrated to suppress phase separation of the host matrix while increasing the efficiency and operational lifetime of deep-blue phosphorescent organic light-emitting diodes (PHOLEDs) with chromaticity coordinates of (0.14, 0.15). The bulky host enables homogenous mixing of the molecules comprising the emissive layer while suppressing single host aggregation; a significant loss channel of nonradiative recombination. By controlling the amorphous phase of the host-matrix morphology, the mixed-host device achieves a significant reduction in nonradiative exciton decay, resulting in $120 \pm 6\%$ increase in external quantum efficiency relative to an analogous, single-host device. In contrast to single host PHOLEDs where electrons are transported by the host and holes by the dopants, both charge carriers are conducted by the mixed host, reducing the probability of exciton annihilation, thereby doubling of the deep-blue PHOLED operational lifetime. These findings demonstrate that the host matrix morphology affects almost every aspect of PHOLED performance.

1. Introduction

The photoluminescent quantum yield (PLQY) of a dopant is a function of its optical properties^[1–3] and morphological^[4] environment. That is, the PLQY is critically affected by molecular aggregation that can lead to increased exciton quenching or triplet–triplet and triplet–polaron annihilation (TTA and TPA, respectively).^[5–9] Increasing the average intermolecular distance of dopant molecules by reducing the dopant aggregation is known to increase the PLQY,^[10] thereby improving the organic light-emitting device (OLED) efficiency, especially at high exciton densities where annihilation dominates.^[7] Although researchers have studied degradation mechanisms related to the thermal stability, host-aggregation and host–guest phase separation in green and red emitting phosphorescent OLEDs (PHOLEDs),^[4,11–16] few studies have dis-

cussed the host aggregation as an origin of annihilation in blue PHOLEDs, especially those that commonly employ the bipolar-conducting host, 3,3'-di(9H-carbazol-9-yl)-1,1'-biphenyl (mCBP).^[16] Homogeneous mixing of the molecules within the emissive layer reduces host-aggregation, and improves exciton confinement in dopants, and thus is critical for improving the device performance.

In this work, we show that the host-matrix amorphous phase improves EQE and operational lifetime of mixed host PHOLEDs by reducing nonradiative quenching at host aggregates found in analogous single host devices. For this purpose, we fabricate PHOLEDs with a mixed emissive layer comprising mCBP and 9,9'-(6-(3-(triphenylsilyl)phenyl)-1,3,5-triazine-2,4-diyl) bis(9H-carbazole) (SiTrzCz2) that features a triphenylsilane group with a glass transition temperature of $T_g = 118 \text{ }^\circ\text{C}$, which is higher than that of mCBP ($T_g = 91 \pm 1 \text{ }^\circ\text{C}$). Addition of this second compound increases the morphological stability by suppressing host crystallization at elevated temperatures. It also leads to homogeneous mixing of the several emissive layer components, including the deep-blue phosphor, fac-tris(5-(tert-butyl)-1,3-diphenyl-2,3-dihydro-1H-imidazo[4,5-b]pyrazine)iridium] ($\text{Ir}(\text{cb})_3$) with chromaticity coordinates of (0.14, 0.15). The suppressed aggregation, in turn, decreases exciton quenching on the phosphorescent molecules that otherwise occurs even at low current densities.^[8,9] The optimized 1:1 volume ratio of mCBP in SiTrzCz2 leads to a $120 \pm 6\%$ relative


H. Zhao, Y. Li, S. R. Forrest
Department of Physics
University of Michigan
Ann Arbor, MI 48109, USA
E-mail: stevefor@umich.edu

J. Kim,^[†] S. R. Forrest
Department of Electrical and Computer Engineering
University of Michigan
Ann Arbor, MI 48109, USA

K. Ding, H. Ade
Department of Physics
North Carolina State University
Raleigh, NC 27695, USA

M. Jung, J. Y. Lee
School of Chemical Engineering
Sungkyunkwan University
Suwon, Gyeonggi 03063, Republic of Korea

S. R. Forrest
Department of Materials Science and Engineering
University of Michigan
Ann Arbor, MI 48109, USA

 The ORCID identification number(s) for the author(s) of this article can be found under <https://doi.org/10.1002/adma.202210794>.

^[†]Present address: Department of Integrated Display Engineering, Yonsei University, 50 Yonsei-ro, Seodaemun-gu, Seoul 03722, Republic of Korea

DOI: 10.1002/adma.202210794

increase in the peak external quantum efficiency (EQE) compared to an emission layer comprising only mCBP. The operational lifetime of the mixed host device is doubled compared to the single host device, showing $LT_{70} = 52 \pm 3$ h versus 24 ± 4 h. Here, LT_{70} is the operation time to reach 70% of initial luminance of $L_0 = 500 \text{ cd m}^{-2}$. Our findings show that the control of the amorphous phase of the host matrix influences several important characteristics of the device performance including charge balance, PLQY, EQE and operational lifetime.

2. Results

The molecular structural formula of SiTrzCz2 is provided in Figure 1a. The optimized structure shows 16° and 19° twist angles of the carbazole and phenyl groups from the center plane, respectively. Density functional theory calculations show that the highest occupied molecular orbital (HOMO) resides primarily on the carbazole, whereas the lowest unoccupied molecular orbital (LUMO) is confined between the triazine and the triphenylsilyl groups at the center of the molecule. Cyclic voltammetry scans give the HOMO energy for SiTrzCz2 of -5.97 eV (see Figure S1 in the Supporting Information). The room temperature UV-vis absorbance spectral onset in Figure 1b shows an optical energy gap of 3.37 eV , from which we infer a LUMO energy $> -2.6 \text{ eV}$. The tetraphenylsilane features a triplet energy $E_T = 3.7 \text{ eV}$, and the carbazole has a HOMO energy of -5.44 eV and $E_T = 3.19 \text{ eV}$.^[17] In SiTrzCz2, the electron polaron is protected by the energy barrier provided by both the triphenylsilyl and carbazole moieties, and the sterically bulky tetrahedral symmetry of the triphenylsilyl moiety. When mixed with other compounds, the triphenylsilyl and the isolated LUMO inhibit ordered molecular stacking, thereby reducing intermolecular interactions that enable exciton quenching.^[18,19] Ir(cb)₃ has a triplet energy of 2.80 eV .^[20] The film phosphorescence spectral onset is 3.04 eV at 77 K , making SiTrzCz2 a suitable host for deep-blue phosphorescent emitters.

Figure 2 shows the phase diagram of films comprising several weight ratios of mCBP and SiTrzCz2 as obtained from differential scanning calorimetry (DSC) data in Figure S2 (Supporting Information) and Table 1. The glass transition temperature, T_g , increases with SiTrzCz2 fraction, from $91 \pm 1^\circ \text{C}$ at $0 \text{ wt}\%$ to $118 \pm 1^\circ \text{C}$ at $100 \text{ wt}\%$ SiTrzCz2. The crystallization temperature of the film, T_c , also increases with SiTrzCz2 concentration. Note that the heat evolved during crystallization decreases with SiTrzCz2 concentration, approaching zero between 55 and $90 \text{ wt}\%$ SiTrzCz2 in mCBP, since material mixing completely suppresses crystallization. Mixing materials also affects the melting temperature, T_m , showing the sharpest melting peak with the most intense heat absorption in the pure mCBP film in Figure S2 (Supporting Information), whereas the peak broadens and decreases with increasing SiTrzCz2 fraction.

Figure 3 shows grazing-incidence wide-angle X-ray scattering (GIWAXS) patterns of layers comprising SiTrzCz2 (Figure 3a), and a mixture of $1:1$ mCBP in SiTrzCz2 (Figure 3b) doped with Ir(cb)₃ at $20 \text{ vol}\%$. Line-cuts of the diffraction patterns of mCBP single and mixed host films are shown in Figure 3c,d, respectively, with their properties summarized in Table 2. The

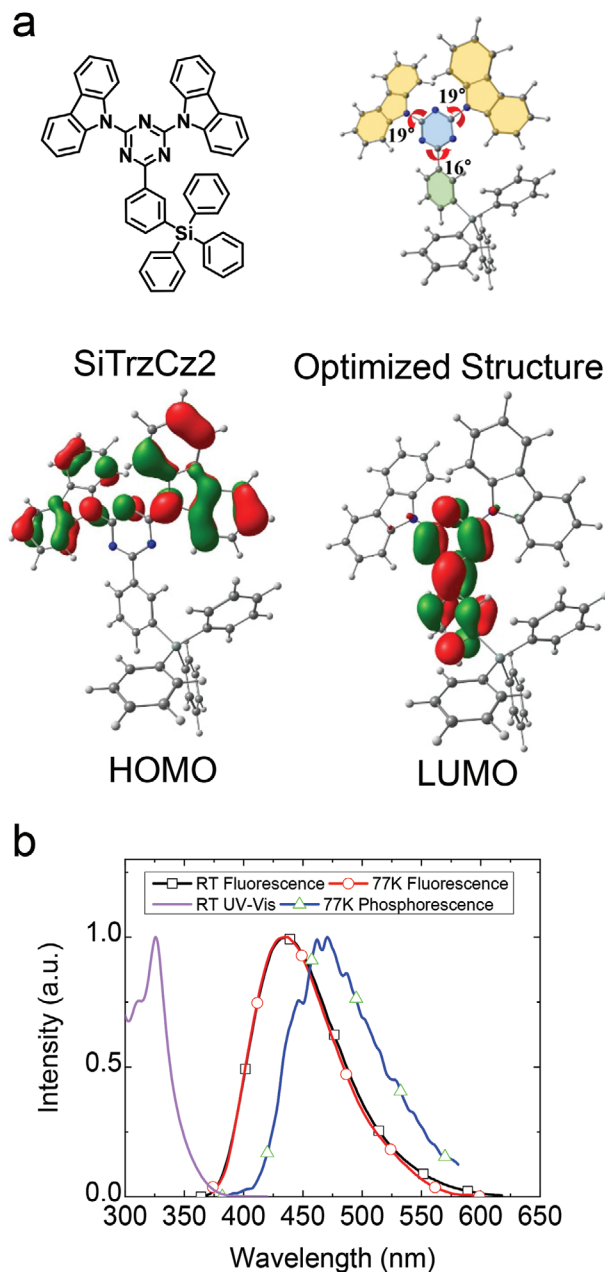


Figure 1. a) Molecular structural formulae of SiTrzCz2 (left) and the calculated optimized structure, and HOMO and LUMO states of SiTrzCz2 via density functional theory (right). b) UV-vis spectra of SiTrzCz2 molecules in tetrahydrofuran (THF) solution at room temperature. Fluorescence and phosphorescence spectra of a neat SiTrzCz2 film at room temperature and 77 K .

r- and *z*-axes correspond to the in- and out-of-plane directions, respectively. The (100) peaks are found at a scattering parameter of $q_z = 0.6 \text{ \AA}^{-1}$, suggesting a lamellar stacking distance of 10.5 \AA . The (010) peak at $q = 1.5 \text{ \AA}^{-1}$ corresponds to a π -stacking distance of 4.2 \AA . The π -stacking habits and lamellar structures of a mCBP molecular crystal are shown in Figure 3e,f, respectively. The mixed film shows two peaks, where the feature at $q = 1.57 \text{ \AA}^{-1}$ possibly arises from π -stacking between the carbazole groups of mCBP and SiTrzCz2. This peak vanishes

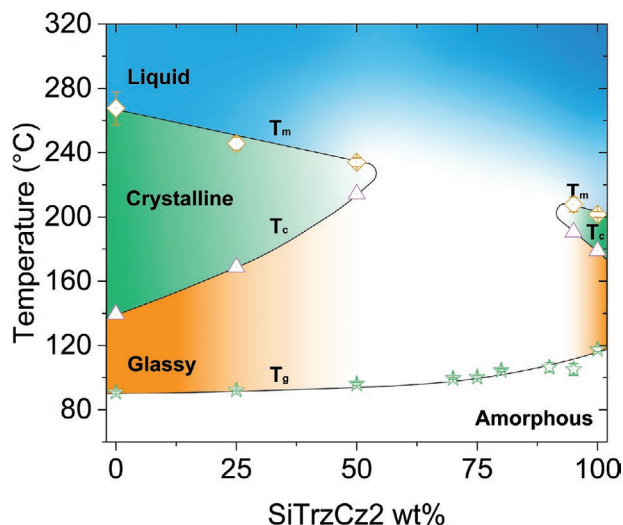


Figure 2. Phase diagram determined by differential scanning calorimetry of mixed films comprising mCBP and SiTrzCz2 at several weight ratios. The trend for each phase transition during the thermal loop is indicated by the solid line. The vanishing boundary between crystal and liquid phases approximately between 55 and 90 wt% SiTrzCz2 is indicated by a white-blue color gradient to show that the mixture stays amorphous during the scan.

with annealing due to weak attraction between mCBP and SiTrzCz2 caused by the bulky structure of SiTrzCz2 (Figure S3, Supporting Information). The full-width-at-half-maximum (FWHM) of the lamellar peak of the mCBP neat and the mixed films are similar. However, the FWHM of the mCBP π -stacking peak increases when SiTrzCz2 is added, from 0.33 ± 0.01 to $0.53 \pm 0.01 \text{ \AA}^{-1}$ for a 1:1 ratio, which indicates that stacking of mCBP is suppressed in the mixture.

Figure 4a shows the proposed energy level scheme of the PHOLED used to study the electroluminescent properties of the mixed host emission layer (EML). Neat layers of *N,N'*-di(1-naphthyl)-*N,N'*-diphenyl-(1,1'-biphenyl)-4,4'-diamine (NPD) and 5-(7-[2,2'-bipyridin]-5-yl)-2-triphenylenyl)-2,2'-bipyridine

Table 1. Differential scanning calorimetry data of films comprising mCBP and SiTrzCz2 at varied doping concentrations.

	Glass transition temperature [T_g] ^{a)}	Crystallization temperature [T_c] ^{b)}	Melting temperature [T_m] ^{a)}
Pure mCBP	$91 \pm 1 \text{ }^\circ\text{C}$	$130 \pm 3 \text{ }^\circ\text{C}$	$268 \pm 10 \text{ }^\circ\text{C}$
25% SiTrzCz2	$92 \pm 1 \text{ }^\circ\text{C}$	$159 \pm 1 \text{ }^\circ\text{C}$	$246 \pm 4 \text{ }^\circ\text{C}$
50% SiTrzCz2	$96 \pm 1 \text{ }^\circ\text{C}$	$190 \pm 1 \text{ }^\circ\text{C}$	$234 \pm 3 \text{ }^\circ\text{C}$
70% SiTrzCz2	$100 \pm 1 \text{ }^\circ\text{C}$	–	–
75% SiTrzCz2	$100 \pm 1 \text{ }^\circ\text{C}$	–	–
80% SiTrzCz2	$105 \pm 1 \text{ }^\circ\text{C}$	–	–
90% SiTrzCz2	$107 \pm 3 \text{ }^\circ\text{C}$	–	–
95% SiTrzCz2	$105 \pm 4 \text{ }^\circ\text{C}$	$177 \pm 1 \text{ }^\circ\text{C}$	$208 \pm 5 \text{ }^\circ\text{C}$
Pure SiTrzCz2	$118 \pm 1 \text{ }^\circ\text{C}$	$166 \pm 1 \text{ }^\circ\text{C}$	$202 \pm 2 \text{ }^\circ\text{C}$

^{a)} T_g and T_m are extracted from the onset temperatures of the DSC curves; ^{b)} T_c is extracted from the recrystallization peak position.

(BPyTP2) are used as the hole and electron transporting layers, respectively, while neat mCBP and SiTrzCz2 are the electron and exciton blocking layers, respectively. The emissive layer is comprised of a mixture of mCBP and SiTrzCz2 doped with Ir(cb)₃. The HOMO levels of the two hosts are comparable, whereas the LUMO energy of SiTrzCz2 is 0.2 eV deeper than that for mCBP. The LUMO energy of SiTrzCz2 is estimated from the energy gap obtained via the UV-vis spectra and the HOMO energy is obtained via cyclic voltammetry. Figure 4b (left) illustrates the proposed mechanisms leading to nonradiative quenching by the mCBP aggregates in the single host device. This includes TTA assisted by the triplet diffusion on host aggregates, and TPA between the dopant triplet and a polaron on the aggregates. The aggregation leads to enhanced diffusion lengths of both excitons and polarons, leading to higher rates of annihilation.^[21,22] In addition, host aggregation leads to phase separation of the host and the dopant molecules, resulting in an enhanced TTA and TPA. On the other hand, quenching is suppressed in the absence of host clustering by blending SiTrzCz2 in mCBP, as shown in Figure 4b (right).

Figure 4c shows the EQE versus current density (J) of the PHOLEDs with a neat mCBP host, and a 1:1 SiTrzCz2:mCBP mixed host for several Ir(cb)₃ doping concentrations. Devices with the mixed host show higher peak EQEs compared to the mCBP single host device at all Ir(cb)₃ concentrations. A maximum EQE = $22 \pm 1\%$ of the mixed host with 12 and 20 vol% Ir(cb)₃ is observed, whereas the neat mCBP host device shows a $56 \pm 4\%$ decrease when the doping concentration is reduced to 12 vol%. The electroluminescence spectra at several J are provided in Figure 4d, with the peak at 465 nm leading to deep-blue 1931 Commission Internationale d'Eclairage (CIE) chromaticity coordinates of (0.14, 0.15), independent of J .

Figure 5a shows the maximum EQE of the PHOLEDs and the PLQY of the emissive layers with 0–90 vol% mixing ratio of SiTrzCz2 in mCBP, and with 20 vol% Ir(cb)₃, indicating maximum at a 1:1 ratio. Figure 5b gives the exciton radiative PL lifetime and PLQY versus Ir(cb)₃ concentration in a mCBP and 1:1 mCBP:SiTrzCz2 host (see Figure S4 in the Supporting Information for more details). The radiative lifetime and PLQY peak at 20 vol% concentration of Ir(cb)₃ in both neat mCBP and 1:1 mixed host films, and decrease at 40 vol%. Figure 5c,d shows the transient electroluminescence (TrEL) of devices comprised of neat mCBP and 1:1 mCBP:SiTrzCz2 with 20 vol% Ir(cb)₃. The mixed host device shows an accelerated TrEL decay with J increasing from 10 mA cm^{-2} to 10 A cm^{-2} , whereas the mCBP-only device shows almost no dependence of lifetime on current. Moreover, the TrEL exciton lifetime of the mixed host approaches that of the neat host device only at the highest current densities ($J = 1\text{--}10 \text{ A cm}^{-2}$). From this, we infer that the nonradiative pathways in the neat mCBP EML are almost fully saturated even at the lowest currents, which is strikingly different from the mixed host case. The time-resolved EL and PL lifetimes are summarized in Figure 5e. Figure 5f compares the relative EQE and the lifetimes of the mixed host device, with a fit to a model discussed in the following section.

Figure 6a,b shows the J versus voltage (V) characteristics of electron- and hole-only devices at several Ir(cb)₃ concentrations in the mixed host EML (for device structures,

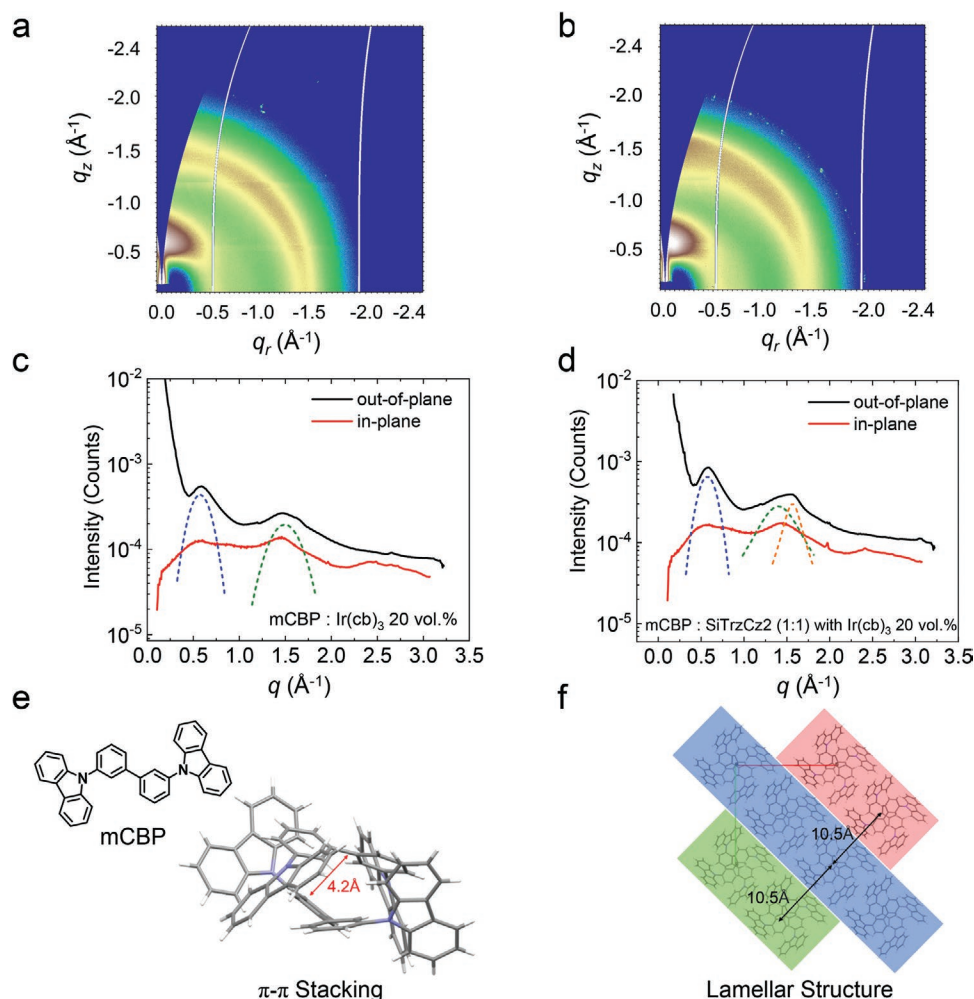


Figure 3. a,b) Grazing-incidence wide-angle X-ray scattering pattern (GIWAXS) of mCBP single host (a) and 1:1 mixed film comprising mCBP and SiTrzCz2 (b). c,d) Line-cut plots of the GIWAXS patterns of mCBP single host (c) and 1:1 mixed film (d). The blue dashed lines are fits to the lamellar peaks, and green/orange lines are fits to the π - π stacking peaks. The 4.2 Å distance between each π -system is shown. Also shown is the molecular structural formulae of mCBP. f) Crystal structure of mCBP showing its lamellar stacking habit. The distance between each lamellar block (10.5 Å) is shown.

see Experimental Section). The current densities for both devices are independent of dopant concentration, indicating that charge is conducted entirely by the hosts rather than the dopant. Since the LUMO of SiTrzCz2 is 0.2 eV deeper than mCBP, we infer that SiTrzCz2 carries electrons in the EML, whereas mCBP conducts holes.^[20] The electrons are blocked by the neat mCBP layer, improving the charge balance. In the

emissive layer comprising a neat mCBP host, the dependence of the current versus Ir(cb)₃ concentration shown in Figure 6c indicates that charges are transported through the dopant in the absence of SiTrzCz2. The similarity of the J - V characteristics and their independence of doping concentration (12–40%) in Figure 6d indicate that charges are only carried by the 1:1 mCBP:SiTrzCz2 blend.

Table 2. Crystal structures of mCBP and 1:1 mixed mCBP:SiTrzCz2 films doped with 20 vol% Ir(cb)₃.

		Location [\AA^{-1}]	Stacking Distance [\AA]	FWHM [\AA^{-1}] ^{a)}	Orientation
Neat mCBP	π - π Stack	1.50	4.21	0.33 ± 0.01	Isotropic
Neat mCBP	Lamellar	0.62	10.14	0.24 ± 0.01	Out-of-plane
Mixed	π - π Stack1	1.57	4.02	0.14 ± 0.01	Out-of-plane
Mixed	π - π Stack2	1.47	4.27	0.53 ± 0.01	Isotropic
Mixed	Lamellar	0.60	10.50	0.24 ± 0.01	Out-of-plane

^{a)} Calculation based on Gaussian fitting model, Fit error = ± 0.01 Å.

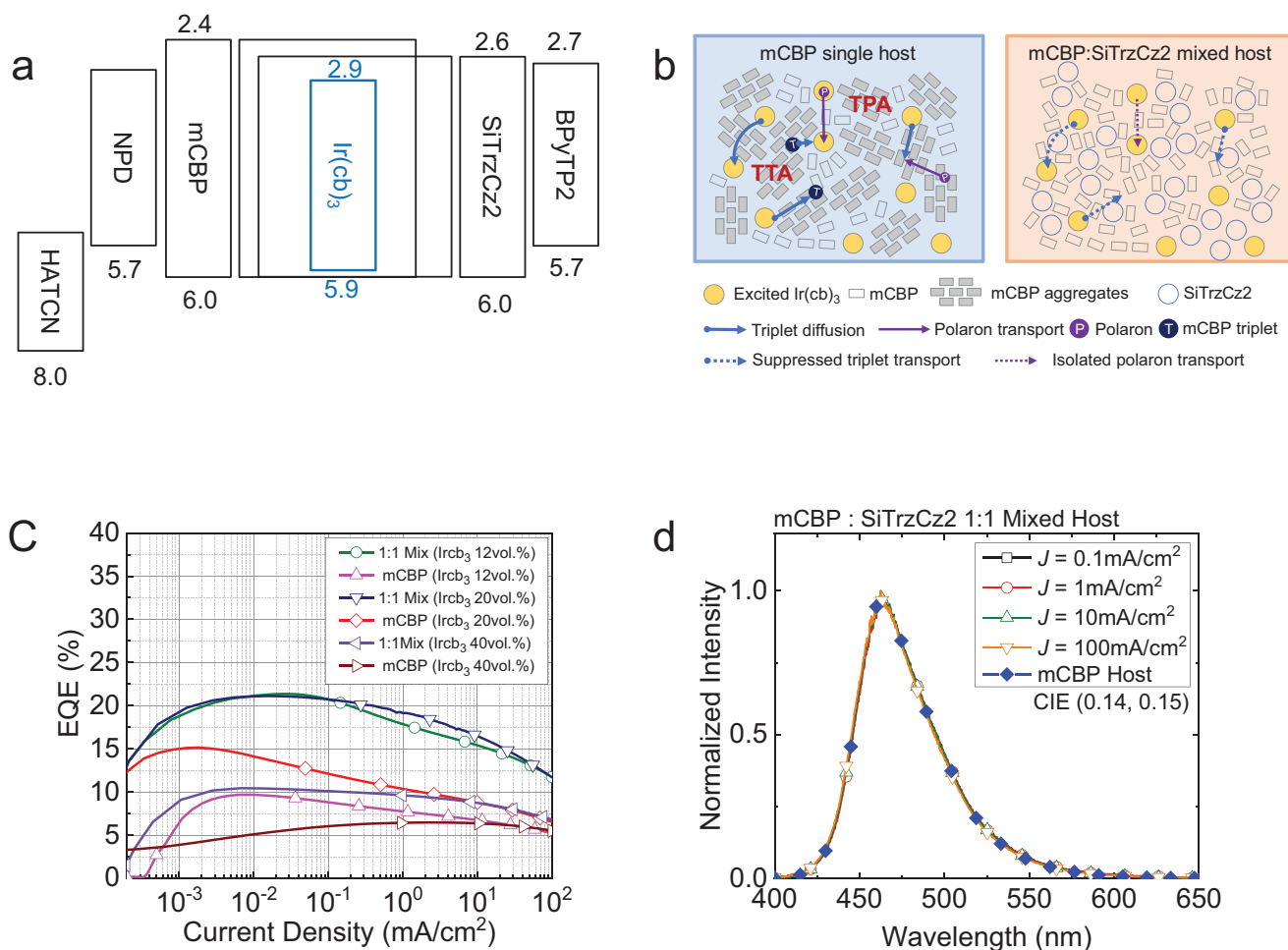


Figure 4. a) Structure of the PHOLED with the frontier orbital energies of the materials in eV. The anode and cathode are located on the left and right sides of the diagram, respectively. b) Illustration of triplet–triplet and triplet–polaron annihilation processes in the mCBP host emissive layer (left) and the suppressed processes in the mCBP:SiTrzCz2 mixed host layer. c) Current density–external quantum efficiency (J -EQE) characteristics of the OLEDs with single and mixed host matrices with various phosphor doping concentrations. d) Electroluminescence spectra of the mixed host device with 12 vol% doped Ir(cb)₃ at several current densities. The blue diamonds show the spectrum of a mCBP single host OLED with a 12 vol% doping concentration of Ir(cb)₃ in the emissive layer.

3. Discussion

The phase diagram in Figure 2 demonstrates that mixing SiTrzCz2 into mCBP stabilizes the morphology of the emissive layer by increasing T_g and T_c with an increasing fraction of SiTrzCz2 from 0% to 50%.^[11,23] As the film is more uniformly blended, it becomes increasingly difficult for the solid to crystallize. Thus, there is no clear region from 55 to 90 wt% SiTrzCz2 that distinguishes between the crystalline and liquid phases. The GIWAXS data in Figure 3 also suggest that mixing mCBP with bulky SiTrzCz2 suppresses aggregation of mCBP, resulting in a broadening of the mCBP π - π stacking peak, and an increased EQE (see Figure 5a).

Uniform mixing is optimized when mCBP and SiTrzCz2 are blended at a 1:1 volume ratio, and the PLQY decreases with the increased concentration of either host, showing the same trend as the amorphous phase in Figure 2. The PLQY and peak EQE of the mixed host are found to surpass those in either neat host matrixes. This indicates that the nonradiative dissipation is determined by both the host mixture ratio as well as

the resulting morphology. Thus, both the high EQE and PLQY are due to improved charge and energy transfer in the blend. The host blend increases the radiative lifetime by limiting quenching in the host-dopant matrix and, consequently, the PLQY of Ir(cb)₃, as shown in Figure 5b. Combining the PLQY and transient PL results, we infer that the nonradiative decay rate is reduced by a factor of four via mixing, as discussed in Figure S5 in the Supporting Information.

We have also found that differences in outcoupling efficiency do not contribute significantly to the increase in EQE with blending ratio, and all devices can reach the same optimal charge balance shown by comparing the peak EQE and PLQY. The outcoupling efficiency is affected by the orientation of the transition dipole moments (TDM) of the dopant. However, the isotropic symmetry of Ir(cb)₃ results in similarly isotropic TDM orientation for the five EMLs with the structures in Figure 5a, as confirmed by the Fourier plane images^[24] of the PL spectra in Figure S10 in the Supporting Information. Additionally, in Figure S11 (Supporting Information), the ratio of EQE_{max}/PLQY from Figure 5a gives

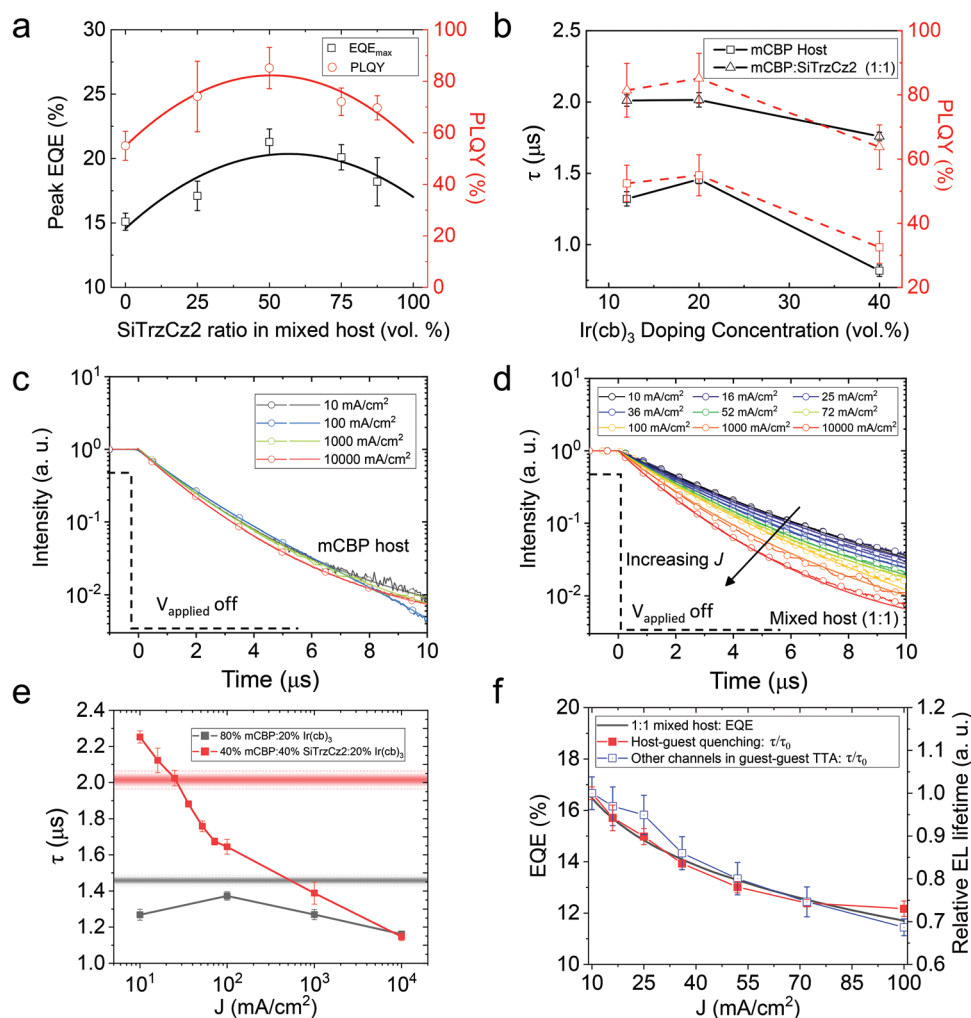


Figure 5. a) Measured photoluminescent quantum yield (PLQY) (red) and peak external quantum efficiency (EQE, black) versus concentration (volume %) of SiTrzCz2 within the emissive layer. b) Measured thin film PLQY (red) and exciton radiative lifetime (black) of the mCBP single host and 1:1 mixed host versus doping concentration of Ir(cb)₃. c,d). Transient electroluminescence (TrEL) and host–guest quenching fitting results to Equations (1) and (2) in text of the mCBP and 1:1 mixed host devices versus current density. The fitting shows a $\tau_Q = 5.5 \pm 0.6 \mu\text{s}$ and $k_r = 0.3 \pm 0.1 \mu\text{s}^{-1}$ in both devices. e) Exciton EL lifetime fit by the host–guest quenching model are shown. For reference, the PL lifetimes for both EMLs are indicated in the gradient red and gray zones, respectively. f) EQE versus relative EL lifetime of the mixed host device ranging from 10 to 100 mA cm⁻². Both the linear decay rate fit by the host–guest quenching model and guest–guest TTA model are shown. EL lifetimes are normalized to 10 mA cm⁻² (see Section S6 for more details in the Supporting Information).

the product of the charge balance factor and outcoupling efficiency. The deviation of this product for host matrixes with various mixing ratios is <4%. The similarity in shape between PLQY and PL lifetime suggests that concentration quenching is negligible for doping ratios from 12% to 20% in both host-matrixes.^[25,26]

To further study the effect of morphology on device performance, we measured the TrEL spectra versus current density.^[4,27] As shown in Figure 5c, The mCBP device EL transients are independent of current density from 10 to 10000 mA cm⁻². Over the same range, the EL lifetime of the mixed-host device decreases from 2.3 to 1.1 μs (Figure 5d). The triplet dynamics can be understood with the coupled equations^[5]

$$\frac{dT(J_0, t)}{dt} = -[k_r + k_{QT}Q(J_0, t)]T(J_0, t) \quad (1)$$

and

$$\frac{dQ(J_0, t)}{dt} = -\frac{1}{\tau_Q}Q(J_0, t) \quad (2)$$

where $Q(J_0, t)$ is the concentration of triplets and/or polarons on host molecules that quench radiative triplets on the dopants, $T(J_0, t)$ (see Figure 4b), and J_0 is the steady state current density. The triplet radiative decay rate is k_r , and the bimolecular quenching rate is k_{QT} ^[6] and τ_Q is the residence time of the excited states on the host molecules. If τ_Q equals the lifetime of the dopant triplet, $T(J_0, t)$ and $Q(J_0, t)$ describe the same dopant triplet species. The equations then correspond to guest–guest TTA, with $k_{QT} = \frac{1}{2}k_{TTA}$. If τ_Q is longer than the natural lifetime of the dopant triplet, the equations describe the TTA following triplet or polaron diffusion in the host aggregates, as illustrated

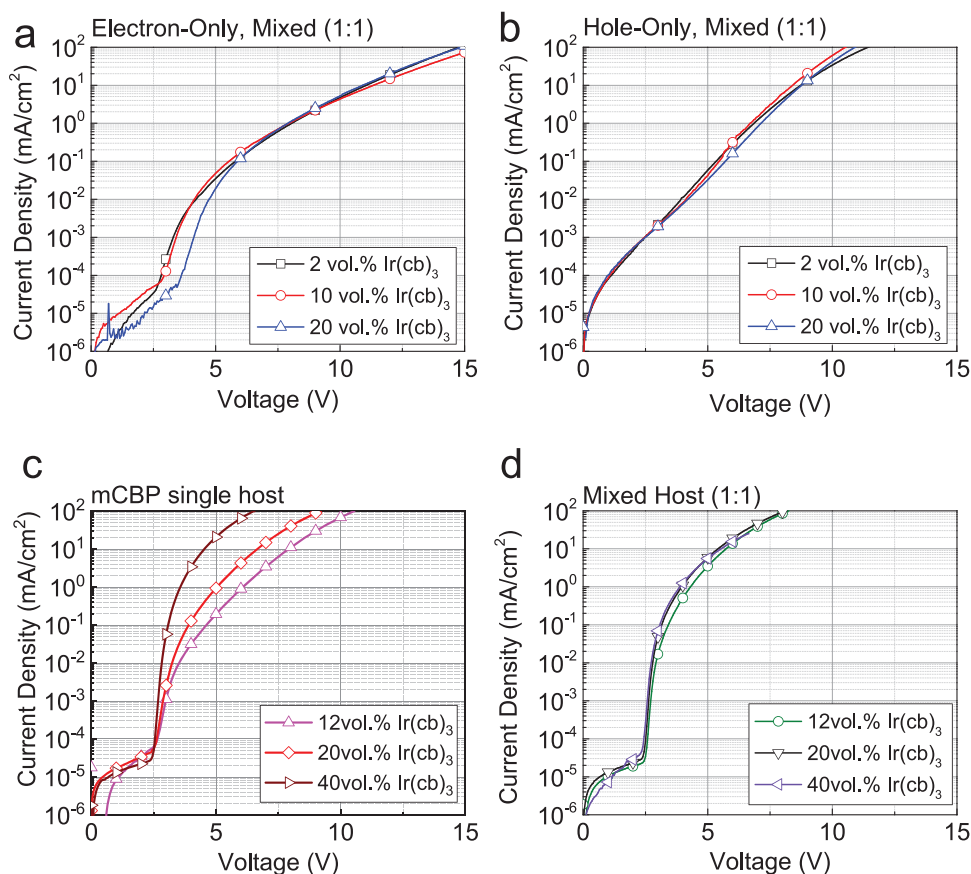


Figure 6. a,b) J - V characteristics of the electron-only (a) and hole-only (b) devices comprising a 1:1 volume ratio mCBP:SiTrzCz2 host at various Ir(cb)₃ concentrations. c,d) J - V characteristics of PHOLEDs with the neat mCBP (c) and 1:1 mixed host (d) at several Ir(cb)₃ concentrations.

in Figure 4b. Since triplets and polarons have different lifetimes on dopants and hosts, τ_Q is the average residence time for the excited states that eventually quench the radiative triplet $T(J_0, t)$. A single exponential decay is obtained for $\tau_Q \rightarrow \infty$ due to long-lived host triplets, polarons, or trap states. Figure 5c,d shows fits to the EL transients with $\tau_Q = 5.5 \pm 0.6 \mu\text{s}$, showing quenching delayed by triplet or polaron diffusion.

The EL intensity is proportional to $T(J, t)$, viz. $L(J_0, t)/L(J_0, 0) = T(J_0, t)/T(J_0, 0)$. Consequently, the quantum yield is proportional to the dopant triplet lifetime via $\Phi(J_1)/\Phi(J_2) = \tau_1/\tau_2$ (see Section S6 in the Supporting Information). In steady state, nonradiative excited states reach a density of $Q = Q(J_0, 0)$. For $\tau = [k_r + k_{QT}Q(J_0, 0)]^{-1}$, we find the dopant triplet lifetime for the 20% doped mixed host device in Figure 4c fits the EQE roll-off data from 10 to 100 mA cm⁻² in Figure 5f. In the conventional TTA model, the nonradiative decay rate, k_{nr} , is due to monomolecular and bimolecular recombination processes,^[5,28] aside from the guest-guest TTA. If guest-guest TTA were significant, this effect should also be present in the neat mCBP device at the same current density, which is contrary to observation in Figure 5c from 10 to 100 mA cm⁻². Our findings suggest that host-guest quenching is significant in neat mCBP, and is suppressed in mixed host devices.

From the foregoing, both models suggest that exciton quenching with the host aggregates dominates the nonradiative

decay rate, leading to the observed roll-off in EQE. This is supported by GIWAXS data where we find that SiTrzCz2 frustrates mCBP aggregation, thereby reducing the triplet diffusion or polaron trapping in mCBP, resulting in a significant improvement in PLQY. At the highest current densities (1–10 A cm⁻²), the host-guest quenching sites are saturated, thus increasing the proportion of guest-guest TTA (Figure S6-1d, Supporting Information). The EL lifetime of the mixed host device is decreased and approaches that of the mCBP host EL lifetime, showing that the exciton quenching in mixed hosts is reduced in comparison to the single host EML. Thus, both the PLQY and TrEL data show a correlation between the amorphous phase of the host-matrix and reduction of the diffusion-limited quenching in mCBP aggregates.

Mixed hosts release dopant molecules from carrying charges while promoting charge balance regardless of the dopant concentration, once the frontier energy levels of the dopant and hosts are aligned,^[29–31] i.e., the HOMO energy of the dopant is aligned with that of the hole-transporting host, as well as the LUMO energy of the dopant and that of the electron-transporting host. As shown in Figure 6c, the conductivity increases with increasing Ir(cb)₃ concentration in neat mCBP devices. By comparison, the J - V characteristics of the mixed host devices in Figure 6d are almost independent of Ir(cb)₃ concentration. The improvement of charge balance is shown by comparing

the peak EQE of the single and mixed host devices with different doping concentrations in Figure 4c. Although the PLQYs are similar (see Figure 5b), the peak EQE is $56 \pm 4\%$ higher at 20 vol% Ir(cb)₃, showing that charge balance is dependent on doping concentration. In contrast, with SiTrzCz2:mCBP, the EQEs for both 12 and 20 vol% doped samples are unchanged, and have a maximum at 22%.

Previously, a PHOLED comprising a 1:1 mCBP and an analog host to SiTrzCz2, i.e., 9-(4-phenyl-6-(3-(triphenylsilyl)phenyl)-1,3,5-triazin-2-yl)-9H-carbazole (SiCzTrz) mixed with 20% Ir(cb)₃ was reported to achieve EQE = 20.3%.^[20] The exothermic energy transfer was attributed to an “electroplex” formed between the host and dopants in an electric field.^[20,32] The electroplex was claimed to be responsible for the high efficiency and long device lifetime. However, we observe a significant change in PLQY at several emissive layer mixing ratios, even though the measurement occurs in the absence of an external electrical field, which rules out the electroplex as a factor in our observations.

PHOLEDs comprising mixed hosts have also previously shown suppressed charge transport by dopant molecules and efficient energy transfer via exciplex formation.^[33,34] The morphological stability achieved by increasing the glass transition temperature has also been studied previously.^[11,35–37] In contrast, our work focuses on suppressed host aggregation and host–guest interactions that lead to reduced nonradiative exciton quenching.^[4] The tunable morphology achieved via blending the host with or without dopants shown in the GIWAXS and DSC measurements implies that this technique can also be applied to other OLED emissive layers comprising homoleptic Ir-complexes or pseudo-octahedral molecules analogous to Ir(cb)₃. The applicability to other geometries, including planar molecules like Pt-phosphors or the linked donor–acceptor configuration employed in thermally activated delayed fluorescence (TADF) molecules remains an open question.^[38–40]

4. Conclusions

A sterically bulky electron-transporting host material, SiTrzCz2 ($T_g = 118$ °C), was added at 1:1 volume ratio with a mCBP co-host in a conventional PHOLED emissive layer. The homogeneous mixing of SiTrzCz2 suppresses the host phase separation, leading to reduced exciton nonradiative quenching and annihilation. Through quantitative analysis of the transient EL and PLQY, we propose that triplet quenching is suppressed by inefficient energy transfer between mCBP aggregates and the dopant triplets. By controlling the amorphous phase of the host-matrix, we have improved the peak EQE of the deep-blue emitting PHOLED by 40–120% compared to a device comprising only a mCBP host, reaching a maximum EQE of $22 \pm 1\%$. Suppressed host–guest nonradiative annihilation reduces the EQE roll-off at high-current densities. The additional SiTrzCz2 carries electrons within the host, whereas mCBP transports holes. Contrary to conventional Ir-based PHOLEDs that conduct holes, the co-host device liberates the dopant from carrying charge. This provides additional degrees of freedom in material choices used for charge conduction and light emission, while reducing

bimolecular interactions in aggregates. These results emphasize the importance of host morphology in the emissive layer for attaining efficient and long-lived deep-blue OLEDs.

5. Experimental Section

Device Fabrication: PHOLEDs were grown on glass substrates with a predeposited and patterned, 70 nm thick ITO anode (Thin Film Devices, Inc.). The ITO-coated substrates were solvent cleaned and then treated in a UV-ozone chamber for 15 min prior to organic film deposition. The organic film layers comprising Al 100 nm/8-quinolinolato lithium (LiQ) 1.5 nm/2,7-di(2,2'-bipyridin-5-yl)triphenylene (BPyTP2) 25 nm/(SiTrzCz2) 5 nm/mCBP:SiTrzCz2:Ir(cb)₃ 50 nm/3,3'-di(9H-carbazol-9-yl)-1,1'-biphenyl (mCBP) 5 nm/N,N'-di(1-naphthyl)-N,N'-diphenyl-(1,1'-biphenyl)-4,4'-diamine (NPD) 5 nm/1,4,5,8,9,11-hexaazatriphenylenehexacarbonitrile (HATCN) 5 nm were grown by vacuum thermal evaporation (VTE) in a chamber with a base pressure of 1×10^{-7} Torr. The devices were patterned using a shadow mask of 2 mm strips for the top Al contacts that defined the 1 mm × 2 mm device active area.

Electron- and hole-only devices were grown on glass substrates as above. The hole-only device structure was Al 100 nm/HATCN 5 nm/mCBP 5 nm/mCBP:SiTrzCz2:Ir(cb)₃ 50 nm/mCBP 5 nm/HATCN 10 nm the ITO substrate. The mCBP neat layers function as a hole transport layer while HATCN facilitates the hole injection from the ITO anode.^[41] Electron-only devices were Al 100 nm/LiQ 1.5 nm/1,3,5-tris(3-pyridyl-3-phenyl)benzene (TmPyPB) 20 nm/mCBP: SiTrzCz2:Ir(cb)₃ 50 nm/TmPyPB 20 nm. The TmPyPB was used to conduct electrons while blocking hole injection via a large energy barrier between the Al contact (work function = 4.08 eV) and the TmPyPB HOMO (6.75 eV), while the 1.5 nm LiQ facilitates the electron injection.^[42] The devices were patterned using a shadow mask of 0.5 mm radius circles for the top Al contacts. Both electron- and hole-only devices used the bottom ITO contact as the anode and the top Al contact as the cathode.

Device Characterization: The J–V and EQE–J characteristics were measured using a parameter analyzer (HP4145, Hewlett–Packard) and a calibrated photodiode (S3584-08, Hamamatsu Photonics) following standard procedures.^[43] The emission spectra were collected via an optical fiber (P400-5-UV-VIS, Ocean Optics, Inc.) positioned at the bottom surface of the substrate. The optical fiber was connected to a calibrated spectrometer (USB4000, Ocean Optics, Inc). For lifetime tests, PHOLEDs were operated at constant current (Agilent, U2722) and the luminance and voltage data were automatically collected (Agilent, 34972A). All devices were encapsulated using glass lids and UV-cured epoxy in the glovebox filled with a pure N₂ atmosphere (<0.1 ppm O₂ and H₂O).

X-ray Diffraction Measurements: Samples for GIWAXS measurements were prepared on Si wafers and thermally annealed in N₂. The samples were measured at Beamline 7.3.3 at the Advanced Light Source (ALS),^[44] Lawrence Berkeley National Laboratory (LBNL). The X-ray energy was 10 keV and the scattering patterns were recorded on a 2D image plate (Pilatus 1 M) with a pixel size of 172 μm (981 × 1043 pixels). The detector was located 300 mm from the sample center, and the incidence angle was 0.13°.

Transient Electroluminescence: Devices were driven by a pulse generator (Agilent, 8114A) with response time <5 ns and stabilized for at least 100 μs. The EL signals were collected by an avalanche photodetector (APD430A2, Thorlabs. Inc) and read out using a 500 MHz digital oscilloscope.

Supporting Information

Supporting Information is available from the Wiley Online Library or from the author.

Acknowledgements

H.Z. and J.K. contributed equally to this work. The work was supported by the U.S. Department of Energy (DOE), Office of Energy Efficiency and Renewable Energy, award No. DE-EE0009688 (J.K., device design). The views expressed herein do not necessarily represent the views of the U.S. Department of Energy or the United States Government. (J.K., H.Z., S.R.F., data collection and analysis) and Universal Display Corporation (J.K., lifetime studies). The authors thank the Lurie Nano Fabrication Facility at the University of Michigan for supporting the device processes. J.Y.L. acknowledges support from the Korean Ministry of Trade, Industry and Energy (20018956). X-ray data acquisition and manuscript preparation by H.A. and K.D. are supported by ONR grant N000142012155. X-ray data were acquired at the Advanced Light Source, which was supported by the Director, Office of Science, Office of Basic Energy Sciences, of the U.S. Department of Energy under Contract DE-AC02-05CH11231.

Conflict of Interest

The authors declare the following competing financial interest(s): S.R.F. has an equity interest in Universal Display Corp. This apparent conflict is under management by the University of Michigan Office of Research. Also, University of Michigan has a license agreement with UDC.

Data Availability Statement

The data that support the findings of this study are available from the corresponding author upon reasonable request.

Keywords

electrophosphorescence, electroplax, morphology, triplet annihilation

Received: November 20, 2022

Revised: December 22, 2022

Published online: February 9, 2023

- [1] M. Furno, R. Meerheim, S. Hofmann, B. Lüssem, K. Leo, *Phys. Rev. B* **2012**, *85*, 115205.
- [2] E. M. Purcell, H. C. Torrey, R. V. Pound, *Phys. Rev.* **1946**, *69*, 37.
- [3] M. A. Fusella, R. Saramak, R. Bushati, V. M. Menon, M. S. Weaver, N. J. Thompson, J. J. Brown, *Nature* **2020**, *585*, 379.
- [4] S. Reineke, G. Schwartz, K. Walzer, M. Falke, K. Leo, *Appl. Phys. Lett.* **2009**, *94*, 163305.
- [5] N. C. Giebink, S. R. Forrest, *Phys. Rev. B* **2008**, *77*, 235215.
- [6] N. C. Giebink, B. W. D'Andrade, M. S. Weaver, P. B. Mackenzie, J. J. Brown, M. E. Thompson, S. R. Forrest, *J. Appl. Phys.* **2008**, *103*, 044509.
- [7] N. C. Giebink, B. W. D'Andrade, M. S. Weaver, J. J. Brown, S. R. Forrest, *J. Appl. Phys.* **2009**, *105*, 124514.
- [8] Y. Divayana, X. W. Sun, *Phys. Rev. Lett.* **2007**, *99*, 143003.
- [9] D. R. Lutz, K. A. Nelson, C. R. Gochanour, M. D. Fayer, *Chem. Phys.* **1981**, *58*, 325.
- [10] S. R. Forrest, *Organic Electronics: Foundations to Applications*, Oxford University Press, Oxford, UK **2020**.
- [11] J. Ràfols-Ribé, P.-A. Will, C. Hänisch, M. Gonzalez-Silveira, S. Lenk, J. Rodríguez-Viejo, S. Reineke, *Sci. Adv.* **2018**, *4*, eaar8332.
- [12] C. Murawski, K. Leo, M. C. Gather, *Adv. Mater.* **2013**, *25*, 6801.
- [13] J.-R. Gong, L.-J. Wan, S.-B. Lei, C.-L. Bai, X.-H. Zhang, S.-T. Lee, *J. Phys. Chem. B* **2005**, *109*, 1675.
- [14] S. K. Shin, S. H. Han, J. Y. Lee, *J. Mater. Chem. C* **2018**, *6*, 10308.
- [15] S. Reineke, G. Schwartz, K. Walzer, K. Leo, *Phys. Status Solidi RRL – Rapid Res. Lett.* **2009**, *3*, 67.
- [16] Y. Zhang, H. Aziz, *ACS Appl. Mater. Interfaces* **2017**, *9*, 636.
- [17] Y. Wang, J. H. Yun, L. Wang, J. Y. Lee, *Adv. Funct. Mater.* **2021**, *31*, 2008332.
- [18] J. Sun, H. Ahn, S. Kang, S.-B. Ko, D. Song, H. A. Um, S. Kim, Y. Lee, P. Jeon, S.-H. Hwang, Y. You, C. Chu, S. Kim, *Nat. Photonics* **2022**, *16*, 212.
- [19] E. Kim, J. Park, M. Jun, H. Shin, J. Baek, T. Kim, S. Kim, J. Lee, H. Ahn, J. Sun, S.-B. Ko, S.-H. Hwang, J. Y. Lee, C. Chu, S. Kim, *Sci. Adv.* **2022**, *8*, eabq1641.
- [20] M. Jung, K. H. Lee, J. Y. Lee, T. Kim, *Mater. Horiz.* **2020**, *7*, 559.
- [21] R. R. Lunt, N. C. Giebink, A. A. Belak, J. B. Benziger, S. R. Forrest, *J. Appl. Phys.* **2009**, *105*, 053711.
- [22] R. R. Lunt, J. B. Benziger, S. R. Forrest, *Adv. Mater.* **2010**, *22*, 1233.
- [23] J. Kwak, Y.-Y. Lyu, S. Noh, H. Lee, M. Park, B. Choi, K. Char, C. Lee, *Thin Solid Films* **2012**, *520*, 7157.
- [24] J. Kim, H. Zhao, S. Hou, M. Khatoniari, V. Menon, S. R. Forrest, *Phys. Rev. Appl.* **2020**, *14*, 034048.
- [25] Y. Kawamura, J. Brooks, J. J. Brown, H. Sasabe, C. Adachi, *Phys. Rev. Lett.* **2006**, *96*, 017404.
- [26] Y. Q. Zhang, G. Y. Zhong, X. A. Cao, *J. Appl. Phys.* **2010**, *108*, 083107.
- [27] Z. Hadidi, M. Ansari-Rad, S. H. Pilehrood, *Appl. Phys. Lett.* **2021**, *119*, 233301.
- [28] S. Reineke, K. Walzer, K. Leo, *Phys. Rev. B* **2007**, *75*, 125328.
- [29] S. Lee, H. Koo, O. Kwon, Y. Jae Park, H. Choi, K. Lee, B. Ahn, Y. Min Park, *Sci. Rep.* **2017**, *7*, 11995.
- [30] H. Shin, S. Lee, K.-H. Kim, C.-K. Moon, S.-J. Yoo, J.-H. Lee, J.-J. Kim, *Adv. Mater.* **2014**, *26*, 4730.
- [31] Y. Zhang, J. Lee, S. R. Forrest, *Nat. Commun.* **2014**, *5*, 5008.
- [32] W. Song, J. Y. Lee, Y. J. Cho, H. Yu, H. Aziz, K. M. Lee, *Adv. Sci.* **2018**, *5*, 1700608.
- [33] Y.-S. Park, S. Lee, K.-H. Kim, S.-Y. Kim, J.-H. Lee, J.-J. Kim, *Adv. Funct. Mater.* **2013**, *23*, 4914.
- [34] S. Lee, K.-H. Kim, D. Limbach, Y.-S. Park, J.-J. Kim, *Adv. Funct. Mater.* **2013**, *23*, 4105.
- [35] J. S. Price, B. Wang, T. Kim, A. J. Grede, J. M. Sandoval, R. Xie, Y. Shen, D. R. Adams, M. J. Eller, A. Sokolov, S. Mukhopadhyay, P. Trefonas, E. D. Gomez, E. A. Schweikert, N. C. Giebink, *Appl. Phys. Lett.* **2018**, *113*, 263302.
- [36] H.-N. Yang, S.-J. He, T. Zhang, J.-X. Man, N. Jiang, D.-K. Wang, Z.-H. Lu, *Org. Electron.* **2018**, *60*, 45.
- [37] J. L. Keddie, R. A. L. Jones, R. A. Cory, *Faraday Discuss.* **1994**, *98*, 219.
- [38] X. Wu, B.-K. Su, D.-G. Chen, D. Liu, C.-C. Wu, Z.-X. Huang, T.-C. Lin, C.-H. Wu, M. Zhu, E. Y. Li, W.-Y. Hung, W. Zhu, P.-T. Chou, *Nat. Photonics* **2021**, *15*, 780.
- [39] M. Sarma, K.-T. Wong, *ACS Appl. Mater. Interfaces* **2018**, *10*, 19279.
- [40] M. Wang, Y.-H. Huang, K.-S. Lin, T.-H. Yeh, J. Duan, T.-Y. Ko, S.-W. Liu, K.-T. Wong, B. Hu, *Adv. Mater.* **2019**, *31*, 1904114.
- [41] J. Niederhausen, P. Amsalem, J. Frisch, A. Wilke, A. Vollmer, R. Rieger, K. Müllen, J. P. Rabe, N. Koch, *Phys. Rev. B* **2011**, *84*, 165302.
- [42] Z. Liu, O. V. Salata, N. Male, *Synth. Met.* **2002**, *128*, 211.
- [43] S. R. Forrest, D. D. C. Bradley, M. E. Thompson, *Adv. Mater.* **2003**, *15*, 1043.
- [44] A. Hexemer, W. Bras, J. Glossinger, E. Schaible, E. Gann, R. Kirian, A. MacDowell, M. Church, B. Rude, H. Padmore, *J. Phys. Conf. Ser.* **2010**, *247*, 012007.